

Engineering Exciton Recombination Pathways in Bilayer WSe_2 for Bright Luminescence

Shiekh Zia Uddin,[#] Naoki Higashitarumizu,[#] Hyungjin Kim, Eran Rabani, and Ali Javey*



Cite This: *ACS Nano* 2022, 16, 1339–1345



Read Online

ACCESS |



Metrics & More



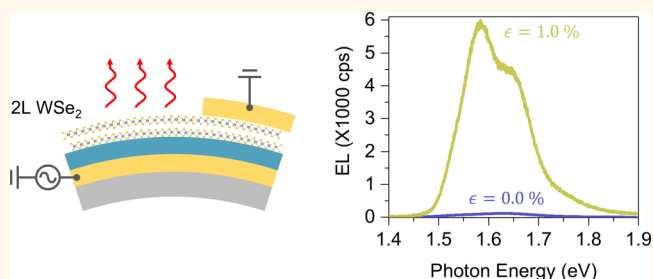
Article Recommendations



Supporting Information

ABSTRACT: Exciton–exciton annihilation (EEA) in counter-doped monolayer transition metal dichalcogenides (TMDCs) can be suppressed by favorably changing the band structure with strain. The photoluminescence (PL) quantum yield (QY) monotonically approaches unity with strain at all generation rates. In contrast, here in bilayers (2L) of tungsten diselenide (WSe_2) we observe a nonmonotonic change in EEA rate at high generation rates accompanied by a drastic enhancement in their PL QY at low generation rates. EEA is suppressed at both 0% and 1% strain, but activated at intermediate strains. We explain our observation through the indirect to direct transition in 2L WSe_2 under uniaxial tensile strain. By strain and electrostatic counterdoping, we attain $\sim 50\%$ PL QY at all generation rates in 2L WSe_2 , originally an indirect semiconductor. We demonstrate transient electroluminescence from 2L WSe_2 with $\sim 1.5\%$ internal quantum efficiency for a broad range of carrier densities by applying strain, which is ~ 50 times higher than without strain. The present results elucidate the complete optoelectronic photophysics where indirect and direct excitons are simultaneously present and expedite exciton engineering in a TMDC multilayer beyond indirect–direct bandgap transition.

KEYWORDS: bilayer WSe_2 , exciton–exciton annihilation, quantum yield, electroluminescence, strain



INTRODUCTION

Recombination in monolayers of transition metal dichalcogenides (TMDCs) is generally dominated by direct transitions; therefore they have received much more attention than their indirect-band-gapped multilayer counterparts.^{1–5} Near-unity photoluminescence (PL) quantum yield (QY) can be achieved in monolayer TMDCs at all generation rates by moving their Fermi level in the middle of the bandgap by electrostatic or chemical counterdoping and changing the band structure favorably by applying strain.⁶ Exciton–exciton annihilation (EEA) is the dominant nonradiative recombination mechanism at high generation rates and is enhanced by van Hove singularities (VHSs) in the density of states (DOS). Application of strain moves the process away from VHSs and monotonically suppresses EEA.⁶

It is desirable to have direct-bandgap thicker TMDCs due to their higher absorptivity and better process stability, but the indirect nature of the multilayer TMDCs limits much of their practical applications in light-emitting devices, photodetectors, and photovoltaics. In contrast to their monolayer counterpart, the photophysics of bilayer TMDCs have not been fully explored quantitatively. Here, first we explore the PL QY of bilayer (2L) WSe_2 as a function of background carrier concentration, generation rate, and band structure. Although the PL QY increases monotonically with strain at low

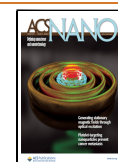
generation rates, we found that the EEA rate changes nonmonotonically at high generation rates. Unlike monolayers, EEA is suppressed at both 0% and 1% strain but activated at intermediate moderate strains. This photophysics is due to an indirect to direct transition that 2L WSe_2 undergoes with moderate uniaxial tensile strain due to a relatively small difference between the direct and indirect bandgap (~ 40 meV).^{7–9}

Three central elements steer the direct exciton recombination mechanism in TMDC monolayers: exciton generation rate, background carrier concentration, and electronic band structure.^{6,10} In bilayer TMDCs, an additional factor, the coexistence of direct and indirect excitons, significantly alters their behavior.^{11–15} Although the indirect-to-direct transition in 2L WSe_2 has been observed before,^{7,8,16} calibrated PL QY was not systematically measured as a function of background carrier concentration and excitation intensity. With optimum electrostatic doping and tensile strain, we achieved $\sim 50\%$ PL

Received: October 19, 2021

Accepted: January 7, 2022

Published: January 11, 2022



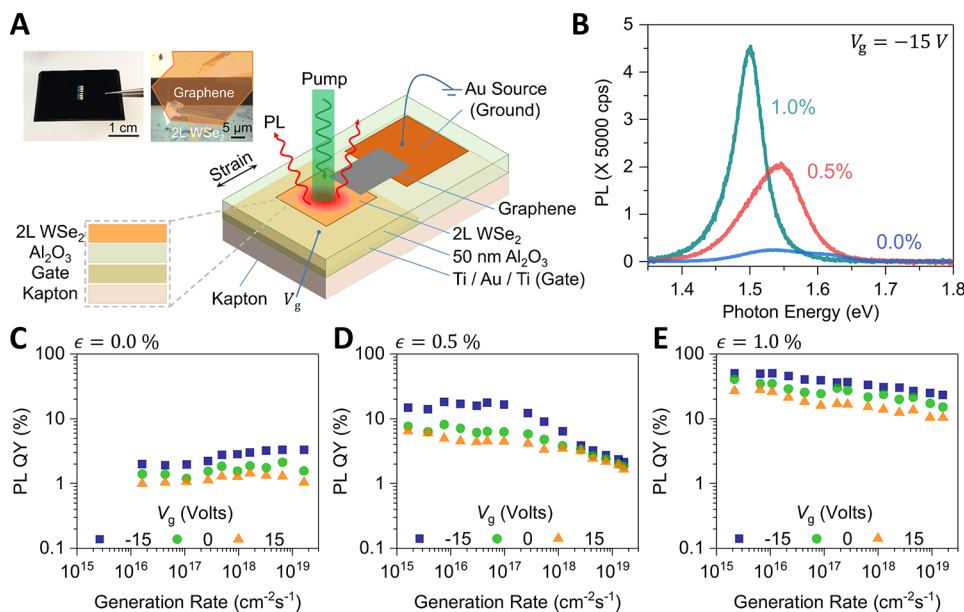


Figure 1. PL QY in 2L WSe₂ at various generation rates and gate voltages. (A) Schematic and optical pictures of the device used to explore the photophysics of 2L WSe₂. (B) PL spectra of the WSe₂ bilayer device under different uniaxial strains of $\epsilon = 0\%$, 0.5% , and 1.0% at a medium generation rate of $G = 10^{17} \text{ cm}^{-2} \text{ s}^{-1}$ and gate voltage of $V_g = -15 \text{ V}$, showing the indirect to direct transition. (C–E) PL QY of bilayer WSe₂ as a function of gate voltage, generation rate, and strain. At $\epsilon = 1.0\%$ strain, $\sim 50\%$ PL QY is achieved.

QY independent of pump intensity in 2L WSe₂, originally an indirect semiconductor. Finally, we demonstrate transient-mode electroluminescence (EL) devices based on 2L WSe₂ with $\sim 1.5\%$ quantum efficiency (QE), which is ~ 50 times higher than without strain. Our results outline the complete optoelectronic photophysics where indirect and direct excitons coexist and instigate exciton engineering in a TMDC multilayer beyond indirect–direct bandgap transition.

RESULTS AND DISCUSSION

Photogenerated carriers in TMDC bilayers form excitons due to strong Coulomb interaction. These excitons can turn into trions in the presence of background carriers, leading to nonradiative recombination. We tune the background carrier concentration (electron and hole population densities) of a 2L WSe₂ by varying the back-gate voltage (V_g) in a capacitor structure and alter the generation rate (G) by varying the pump laser intensity. Generation rate G is the number of excitons created or the number of photons absorbed per unit area per unit time. Gate electrodes (Ti/Au/Ti) were fabricated on top of a polyimide substrate, used as the strain platform because of its flexibility and process compatibility. A 50 nm thick Al₂O₃ gate oxide was deposited *via* an atomic layer deposition (ALD), followed by fabrication of a source electrode on top of Al₂O₃ (Figure 1A). An as-exfoliated 2L WSe₂ flake (Figure S1) was dry-transferred onto the Al₂O₃ gate oxide and contacted with the source electrode through few-layer graphene intermediation, which acts as a flexible electrode. The applied strain in 2L WSe₂ was estimated from a cross-section optical image, assuming the strain is transferred entirely from a flexible substrate to WSe₂. Figure 1B shows PL spectra under different uniaxial tensile strains at a medium generation rate of $G = 10^{17} \text{ cm}^{-2} \text{ s}^{-1}$ and gate voltage of $V_g = -15 \text{ V}$ (see V_g -dependent spectra in Figure S2). Unstrained 2L WSe₂ shows indirect valley transition at lower energy (Γ_C-K_V) with a shoulder peak at the higher energy corresponding to direct valley transition (K_C-K_V).^{7,9,17} Under a moderate strain

of $\epsilon = 0.5\%$, a single peak is observed with a smaller full-width at half-maximum (fwhm) compared to 0% strain. The fwhm further decreases and a red-shift is observed at a strain of $\epsilon = 1.0\%$, the maximum strain without a brittle fracture of ALD oxide. These results are attributed to the indirect to direct bandgap transition with increasing tensile strain.^{7,8,16}

To further understand the photophysics in the WSe₂ bilayer, calibrated PL measurements were performed, extracting the QY quantitatively as a function of ϵ , V_g , and G (Figure 1C–E). Figure 1C shows V_g and G dependence of PL QY in unstrained 2L WSe₂. At zero and positive gate voltages, the nonradiative negative trion recombination is dominant¹⁸ because of the large background electron concentration resulting in a low PL QY of $\sim 1\%$. At negative gate voltage, radiative recombination of neutral excitons becomes dominant, leading to PL QY enhancement.^{6,10} We note that, at 0% strain, PL QY does not show a significant dependence on generation rate. PL QY increases by 1 order of magnitude at low pump with an application of 0.5% tensile strain due to the indirect–direct transition, whereas PL QY drastically droops at the high generation rate (Figure 1D). In excitonic semiconductors, this droop is caused by exciton–exciton annihilation.^{6,10,19,20} With a tensile strain of 1.0% , PL QY droop is effectively suppressed again at the high generation rate (Figure 1E). With optimum electrostatic doping and tensile strain, we achieved $\sim 50\%$ PL QY in 2L WSe₂ at all generation rates. The EEA suppression observed here is markedly different from that of monolayer WSe₂ under strain, where strain monotonically changes EEA.^{6,18}

The observed spectra and the EEA suppression can be explained from the strain-dependent band structure of 2L WSe₂. The qualitative change in the band structure with strain is illustrated in the schematic of Figure 2A. In an unstrained bilayer, the minimum and maximum energy of the conduction and valence band are at the Γ and K point, respectively, resulting in the lowest energy transition being indirect and of low PL QY. With a sufficient tensile strain, the minimum and

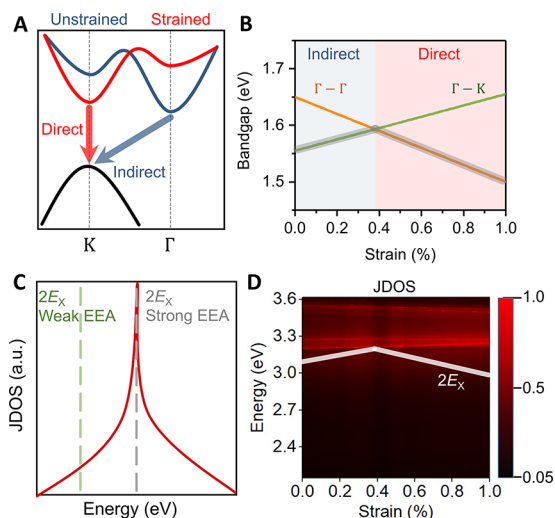


Figure 2. Band structure evolution of 2L WSe₂ under strain. (A) Schematic band structure, qualitatively showing direct to indirect transition of 2L WSe₂ with different strain conditions and under illumination. (B) Calculated energy difference for different transitions of bilayer WSe₂. (C) Schematic illustrating how JDOS at twice the exciton transition energy E_x determines the EEA rate. (D) EEA final energy cusping VHS on the JDOS of bilayer WSe₂.

maximum energy of the conduction and valence band both reside in the K point, making the lowest energy optical transition be direct, thus increasing PL QY. Strain-dependent energy differences of conduction and valence band between Γ points and Γ -K points calculated with density functional theory (DFT) are shown in Figure 2B. We observe the crossover from indirect to direct bandgap at $\epsilon \approx 0.4\%$. Due to the increasing and decreasing nature of direct and indirect energy gaps with strain, respectively, the minimum energy of optical transition, highlighted in gray in Figure 2B, shows a peak at the transition strain. The indirect to direct transition explains the change in PL QY with strain at low generation rate; however we have to look at the joint density of states (JDOS) to understand the change in EEA with strain at high generation rate. During EEA one exciton nonradiatively transfers its energy to another exciton. Momentum and energy conservation dictate that the electron from the energized exciton ends up with a wavevector in which the energy difference between the conduction and valence bands is equal to twice the exciton transition energy $2E_x$. For a direct bandgap excitonic semiconductor, the JDOS at twice the exciton transition energy determines the strength of EEA.^{6,21} Because the Coulomb potential in 2D is inversely proportional to the wavevector of the interacting particles, maximum interaction occurs when they have opposing crystal momentum.²² Therefore, even in indirect semiconductors, the JDOS at twice the exciton transition energy determines the strength of the EEA. If there is a naturally occurring VHS in 2D JDOS at twice the exciton transition energy $2E_x$, strong EEA is observed. On the other hand, if the JDOS is low at $2E_x$, weak EEA is observed (Figure 2C). Figure 2D shows the calculated JDOS of 2L WSe₂ as a function of strain. At around 0.4% tensile strain, the solid curve representing $E = 2E_x$ has a peak maximum touching on a sharply enhanced JDOS of VHSs arising from saddle points in the energy dispersion, which strongly enhances EEA. This explains why no EEA is observed at no strain and $\epsilon = 1.0\%$, but EEA is observed at $\epsilon = 0.5\%$.

The strain dependence of PL QY and EEA in 2L WSe₂ (Figure 1C–E) is well explained by the interplay of the lowest dominant transition and VHS in 2L WSe₂ under strain, both indirect–direct bandgap transition and EEA enhancement by VHS at the intermediate strains. The movement of the direct exciton transition energy away from the VHS at the maximum strain of 1.0% enables PL QY enhancement with no droop at the high generation rate. Figure 3 summarizes the recombi-

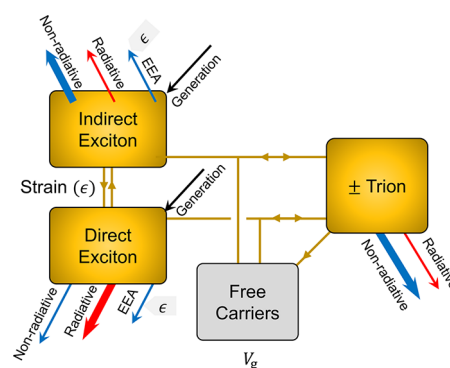


Figure 3. Recombination pathways in 2L WSe₂. Interaction of direct and indirect excitons, trions, and free carriers and their subsequent recombination channels in bilayer WSe₂. Both indirect and direct excitons can turn into trions in the presence of background carriers, which is tuned by gate voltage. Strain controls the ratio of direct and indirect excitons by changing the indirect and direct bandgap and the nonradiative EEA rate by moving the EEA process in and out of resonance. The respective recombination channels of all of these different quasiparticles determine the radiative efficiency.

nation pathways present in 2L WSe₂. Both indirect and direct excitons can turn into trions, which can be controlled by gate voltage. Strain controls both the ratio of indirect and direct excitons and their EEA rates. The interplay of these factors gives rise to the complex photophysics observed in 2L WSe₂.

Time-resolved (TR) PL measurements were performed with changing gate voltage, pump fluence, and strain. At a low initial carrier concentration of $3.3 \times 10^{10} \text{ cm}^{-2}$, unstrained 2L WSe₂ has the longest lifetime of $\sim 0.4 \text{ ns}$ at the negative voltage of $V_g = -15 \text{ V}$ and a shorter lifetime of ~ 0.3 and $\sim 0.07 \text{ ns}$ at $V_g = 0$ and 15 V , respectively (Figure 4A). This gate dependence is consistent with the aforementioned PL QY evolution, indicating that trion nonradiative recombination, whose lifetime is much shorter than trion and exciton radiative lifetimes, is predominant at zero and positive voltage. At the highest initial carrier concentration of $2.7 \times 10^{12} \text{ cm}^{-2}$, TR PL decay shows the same gate dependence as that of low carrier concentration (Figure 4B), and extracted lifetime is almost constant over 3 orders of magnitude variation in the pump fluence (Figure 4C), indicating the absence of EEA. Figure 4D–F show TR PL and extracted lifetime as a function of gate voltage and initial carrier concentration when a tensile strain of 1.0% is applied.^{23,24} No significant change in the lifetime with strain has been observed. Exciton diffusion length is important for understanding the energy transport physics in excitonic semiconductors and a key design consideration in many optoelectronic applications.^{25–27} PL images of 2L WSe₂ excited by a diffraction-limited laser at different generation rates and strain are shown in Figure S3A. Diffusion length is calculated by deconvolving the PL map with laser spot shape and then determining the width of the exciton density profile,

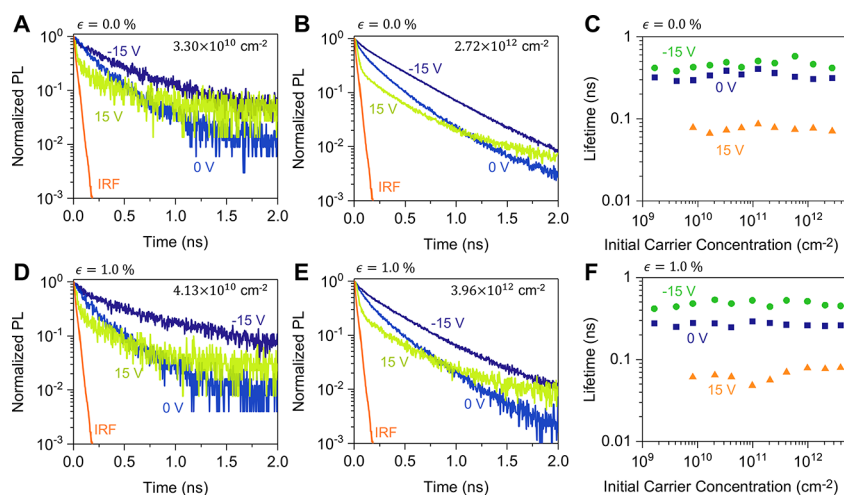


Figure 4. Time-resolved PL of 2L WSe₂. (A, B) Time-resolved PL of 2L WSe₂ as a function of gate at high and low pump fluence at no strain. (C) Extracted initial lifetime at no strain. (D, E) Time-resolved PL of 2L WSe₂ as a function of gate at high and low pump fluence at 1% applied strain. (F) Extracted initial lifetime at 1% applied strain.

as shown in Figure S3B. Unstrained 2L WSe₂ shows larger diffusion length $D_{\text{ex}}^{0\%} \approx 420$ nm, compared to $D_{\text{ex}}^{1\%} \approx 200$ nm observed in the 1% strained bilayer, indicating that the indirect exciton diffuses faster than the direct exciton. This is possibly due to fast radiative lifetime of direct excitons, and further studies are necessary to understand the pump dependence of the diffusion length.

To demonstrate a potential impact of WSe₂ bilayer in the application of light-emitting devices, a transient-mode EL was measured using a bipolar sine wave applied to the gate electrode, while the source electrode is grounded (Figure 5A). Figure 5B shows EL spectra from 2L WSe₂ with and without applying strain at a frequency of $f = 1.0$ MHz and gate voltage of $V_g = 25$ V. A broad peak is observed with applied 0% strain, while EL peak intensity at 1% tensile strain is an order of magnitude higher than that of unstrained. Like the PL spectrum from unstrained 2L WSe₂ (Figure 1B), the strained EL device has two emission peaks at lower and higher energy corresponding to the indirect and direct bandgap transitions, respectively. The discrepancy of the spectrum shapes between PL and EL under the specific strain is probably due to a different built-in strain from device to device *via* poly(methyl methacrylate) (PMMA) transfer or postbaking process or large changes in background carrier concentration during the transient EL process. As a function of operating frequency, the EL intensity monotonically increased with no spectral shape change. The gate voltage dependence was measured with and without applying strain at $f = 1$ MHz (Figure 5C). The turn-on voltage V_{on} was approximately 5.0 and 7.5 V for unstrained and 1.0% strained devices, respectively, which depends on the bandgap of materials, gate capacitance, and parasitic resistances.^{28,29} An order of magnitude EL enhancement was confirmed after the device was turned on over $V_g = 10$ V.

To further quantitatively compare the brightness of 2L WSe₂ with previously reported TMDC EL devices,^{28,29} we extracted internal QE from EL measurement under various measurement conditions of gate voltage, frequency, and strain. The total number of carriers injected ($n_0 + p_0$) in a field-effect transistor when the gate voltage is swept from $-V_g$ to $+V_g$ is given by

$$n_0 + p_0 = C_{\text{ox}}(2V_g - E_g)/q$$

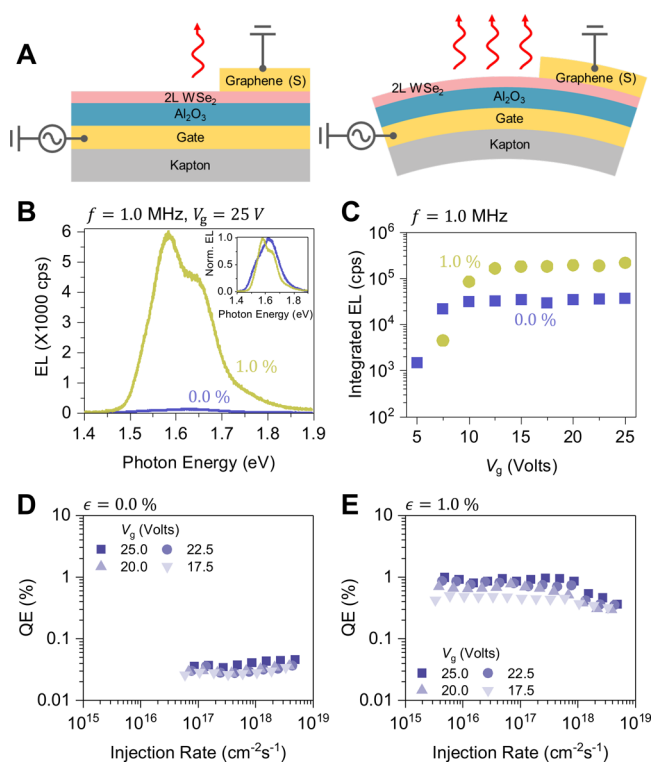


Figure 5. Electroluminescence from 2L WSe₂. (A) Schematics of strain-tunable transient mode EL device. (B) EL spectra of the EL device with and without strain. (C) Integrated EL intensity as a function of V_g at $f = 1.0$ MHz showing device turn on. (D, E) Internal QE of EL device as a function of injected carrier density under different ϵ and V_g .

where n_0 and p_0 are the steady-state electron and hole concentrations corresponding to a positive and negative V_g , respectively, C_{ox} is the areal gate capacitance, and q is the elementary charge. When a periodic signal of frequency f is applied across the device, this transition takes place at f times per second. Therefore, the injection rate Q can be written as

$$Q = f(n_0 + p_0)$$

Taking the ratio between the output EL photons per unit seconds to the injection rate gives us the quantum efficiency. Figure 5D,E show the dependence of EL QE for 2L WSe₂ on injected carrier density at different V_g and strain. The unstrained device exhibits an EL QE of approximately 0.03% at maximum, which is comparable to the reported EL QE of $\sim 0.06\%$ in as-exfoliated monolayer WSe₂.²⁸ With applying a tensile strain of 1.0%, the EL QE drastically increases by over 10 times compared to the no strain device. Notably, the efficiency roll-off was effectively suppressed at the high carrier density, indicating reduced nonradiative recombination. The highest EL QE of 2L WSe₂ reached 1.5%, which is a ~ 50 -fold enhancement compared to the unstrained device. Here, we note that the EL QE is underestimated because the parasitic capacitances are predominant in the current measurement of micrometer-scale devices. Furthermore, the top sublayer in 2L WSe₂ feels a smaller electric field than the bottom layer because of the single-gate structure, leaving room for further improvement of EL performance with utilizing such as dual-gate device structure.³⁰ Further improvement of the EL QE is possible by improving the strain transfer on the emitting bilayer. Although a WSe₂ thicker film can show similar EL enhancement by strain, the trilayer showed poor enhancement compared to the bilayer (Figure S4), probably because of the larger energy difference between direct and indirect bandgap^{7,31} and the experimental limitation in ALD oxide with applicable strain up to 1.0%. Further strain engineering in a multilayer beyond bilayer can be achievable by using two-dimensional heterostructures such as with graphene and *h*-BN.

CONCLUSION

In conclusion, we have demonstrated high PL QY in bilayer WSe₂ at all generation rates with modulating background carrier concentration and electronic band structure *via* strain. Unlike other monolayer and bilayer TMDCs, bilayer WSe₂ experiences the indirect–direct transition and enhanced EEA by VHS resonance at the intermediate tensile strain, making it a direct bandgap and free from EEA above intermediate strain values, resulting in the highest PL QY of $\sim 50\%$ at all exciton densities with applying a 1.0% tensile strain. The observed photophysics is corroborated by DFT calculation of band structure correlating the change in the band structure and VHS on the PL QY. Finally, we showed that the transient mode EL device is based on 2L WSe₂ and a gate with $\sim 1.5\%$ QE, as bright as monolayer EL devices, thus enabling the bilayer to be a promising candidate for light-emitting materials. Our results resolve the complete optoelectronic photophysics when indirect and direct excitons are coexistent and could potentially be a strategy for strain-engineered optoelectronics in multilayered van der Waals semiconductors.

METHODS

Device Fabrication. The PL and EL devices were fabricated on a polyimide substrate (Kapton, Dupont, 1.5 mm thick). Ti (10 nm)/Au (100 nm)/Ti (10 nm) were fabricated as back gate electrodes using standard photolithography and thermal evaporation. As a gate insulator, 50 nm Al₂O₃ was deposited *via* ALD at 200 °C. The 50 nm thick Au source electrodes were patterned on ALD oxide adjacent to gate electrodes. WSe₂ (HQ Graphene) was mechanically exfoliated on a 50 nm SiO₂/Si substrate. Bilayers were identified by optical contrast and AFM height profile. 2L WSe₂ flakes were picked up with PMMA and transferred onto the ALD oxide, followed by a postbaking at 180 °C for 5 min and dichloromethane treatment to remove PMMA. As a source contact, mechanically exfoliated few-layer

graphene (Graphenium, NGS Naturgraphit) was dry-transferred with PMMA to mediate between the Au electrode pad and 2L WSe₂. Another postbaking (180 °C, 5 min) was performed to improve the adhesion between the interfaces of WSe₂/Al₂O₃ and graphene/WSe₂.

Electrical and Optical Characterization. Devices were charged from a Keithley 2410 source meter applied to the gate electrode, while the Au source was grounded. The PL QY was measured using a home-built micro-PL instrument described in detail in a previous study.²³ A 514.5 nm line was used as the excitation source. A uniaxial tensile strain was applied in the 2L WSe₂ by a two-point linear actuator.⁷ The nominal applied strain was calculated using the equation $\varepsilon = t/R$, where $2t$ and R are the substrate thickness and curvature radius measured through the cross-section optical image. TR PL spectra were collected using a time-correlated single photon counting (TCSPC) module. A monochromated line of 514 nm from a supercontinuum laser was used as an excitation source. PL spatial images were measured with a fluorescence microscopy setup using the green laser, the same as the excitation source for PL measurement, acquiring images by a CCD detector (Andor Luca).²⁷ The samples were excited by a green laser, same as the PL measurement, focused to a diffraction-limited spot. EL devices were pumped using a bipolar sine wave from an Agilent 33522A arbitrary waveform generator applied to the gate electrode, while the source contact was grounded. All measurements reported in this paper are taken at room temperature in an ambient lab condition under nitrogen flow.

ASSOCIATED CONTENT

Supporting Information

The Supporting Information is available free of charge at <https://pubs.acs.org/doi/10.1021/acsnano.1c09255>.

Optical and AFM images, PL spectra, PL spatial images, and diffusion length (PDF)

AUTHOR INFORMATION

Corresponding Author

Ali Javey – *Electrical Engineering and Computer Sciences, University of California, Berkeley, California 94720, United States; Materials Sciences Division, Lawrence Berkeley National Laboratory, Berkeley, California 94720, United States; orcid.org/0000-0001-7214-7931; Email: ajavey@berkeley.edu*

Authors

Shiekh Zia Uddin – *Electrical Engineering and Computer Sciences, University of California, Berkeley, California 94720, United States; Materials Sciences Division, Lawrence Berkeley National Laboratory, Berkeley, California 94720, United States; orcid.org/0000-0002-1265-9940*

Naoki Higashitarumizu – *Electrical Engineering and Computer Sciences, University of California, Berkeley, California 94720, United States; Materials Sciences Division, Lawrence Berkeley National Laboratory, Berkeley, California 94720, United States; orcid.org/0000-0003-3996-6753*

Hyungjin Kim – *Electrical Engineering and Computer Sciences, University of California, Berkeley, California 94720, United States; Materials Sciences Division, Lawrence Berkeley National Laboratory, Berkeley, California 94720, United States*

Eran Rabani – *Materials Sciences Division, Lawrence Berkeley National Laboratory, Berkeley, California 94720, United States; Department of Chemistry, University of California, Berkeley, Berkeley, California 94720, United States; The Raymond and Beverly Sackler Center of Computational*

Molecular and Materials Science, Tel Aviv University, Tel Aviv 69978, Israel; orcid.org/0000-0003-2031-3525

Complete contact information is available at:
<https://pubs.acs.org/10.1021/acsnano.1c09255>

Author Contributions

#S.Z.U. and N.H. contributed equally.

Author Contributions

S.Z.U., H.K., N.H., and A.J. conceived the idea for the project and designed the experiments. S.Z.U. and N.H. fabricated devices and performed optical measurements. S.Z.U., N.H., and A.J. analyzed the data. S.Z.U. and E.R. performed analytical modeling. S.Z.U., N.H., and A.J. wrote the manuscript. All authors discussed the results and commented on the manuscript.

Notes

The authors declare no competing financial interest.

ACKNOWLEDGMENTS

This work is supported by the Director, Office of Science, Office of Basic Energy Sciences, Materials Sciences and Engineering Division of the U.S. Department of Energy, under contract no. DE-AC02-05Ch11231. H.K. acknowledges support from Samsung Scholarship. N.H. acknowledges support from the Postdoctoral Fellowships for Research Abroad of Japan Society for the Promotion of Science.

REFERENCES

- (1) Mak, K. F.; Lee, C.; Hone, J.; Shan, J.; Heinz, T. F. Atomically Thin MoS₂: A New Direct-Gap Semiconductor. *Phys. Rev. Lett.* **2010**, *105* (13), 136805.
- (2) Splendiani, A.; Sun, L.; Zhang, Y.; Li, T.; Kim, J.; Chim, C.-Y.; Galli, G.; Wang, F. Emerging Photoluminescence in Monolayer MoS₂. *Nano Lett.* **2010**, *10* (4), 1271–1275.
- (3) Radisavljevic, B.; Radenovic, A.; Brivio, J.; Giacometti, V.; Kis, A. Single-Layer MoS₂ Transistors. *Nat. Nanotechnol.* **2011**, *6* (3), 147–150.
- (4) Wang, Q. H.; Kalantar-Zadeh, K.; Kis, A.; Coleman, J. N.; Strano, M. S. Electronics and Optoelectronics of Two-Dimensional Transition Metal Dichalcogenides. *Nat. Nanotechnol.* **2012**, *7* (11), 699–712.
- (5) Lopez-Sanchez, O.; Lembke, D.; Kayci, M.; Radenovic, A.; Kis, A. Ultrasensitive Photodetectors Based on Monolayer MoS₂. *Nat. Nanotechnol.* **2013**, *8* (7), 497–501.
- (6) Kim, H.; Uddin, S. Z.; Higashitaramizu, N.; Rabani, E.; Javey, A. Inhibited Nonradiative Decay at All Exciton Densities in Monolayer Semiconductors. *Science* **2021**, *373* (6553), 448–452.
- (7) Desai, S. B.; Seol, G.; Kang, J. S.; Fang, H.; Battaglia, C.; Kapadia, R.; Ager, J. W.; Guo, J.; Javey, A. Strain-Induced Indirect to Direct Bandgap Transition in Multilayer WSe₂. *Nano Lett.* **2014**, *14* (8), 4592–4597.
- (8) Ahn, G. H.; Amani, M.; Rasool, H.; Lien, D.-H.; Mastandrea, J. P.; Ager, J. W., III; Dubey, M.; Chrzan, D. C.; Minor, A. M.; Javey, A. Strain-Engineered Growth of Two-Dimensional Materials. *Nat. Commun.* **2017**, *8* (1), 608.
- (9) Sahin, H.; Tongay, S.; Horzum, S.; Fan, W.; Zhou, J.; Li, J.; Wu, J.; Peeters, F. M. Anomalous Raman Spectra and Thickness-Dependent Electronic Properties of WSe₂. *Phys. Rev. B Condens. Matter* **2013**, *87* (16), 165409.
- (10) Lien, D.-H.; Uddin, S. Z.; Yeh, M.; Amani, M.; Kim, H.; Ager, J. W., 3rd; Yablonovitch, E.; Javey, A. Electrical Suppression of All Nonradiative Recombination Pathways in Monolayer Semiconductors. *Science* **2019**, *364* (6439), 468–471.
- (11) Lezama, I. G.; Arora, A.; Ubaldini, A.; Barreteau, C.; Giannini, E.; Potemski, M.; Morpurgo, A. F. Indirect-to-Direct Band Gap Crossover in Few-Layer MoTe₂. *Nano Lett.* **2015**, *15* (4), 2336–2342.
- (12) Brar, V. W.; Sherrott, M. C.; Jariwala, D. Emerging Photonic Architectures in Two-Dimensional Opto-Electronics. *Chem. Soc. Rev.* **2018**, *47* (17), 6824–6844.
- (13) Jariwala, D.; Davoyan, A. R.; Wong, J.; Atwater, H. A. Van Der Waals Materials for Atomically-Thin Photovoltaics: Promise and Outlook. *ACS Photonics* **2017**, *4* (12), 2962–2970.
- (14) Zhang, H.; Abhiraman, B.; Zhang, Q.; Miao, J.; Jo, K.; Roccasceca, S.; Knight, M. W.; Davoyan, A. R.; Jariwala, D. Hybrid Exciton-Plasmon-Polaritons in van der Waals Semiconductor Gratings. *Nat. Commun.* **2020**, *11* (1), 3552.
- (15) Aslan, O. B.; Datye, I. M.; Mleczko, M. J.; Sze Cheung, K.; Krylyuk, S.; Bruma, A.; Kalish, I.; Davydov, A. V.; Pop, E.; Heinz, T. F. Probing the Optical Properties and Strain-Tuning of Ultrathin Mo_{1-x}W_xTe₂. *Nano Lett.* **2018**, *18* (4), 2485–2491.
- (16) Zhao, W.; Ribeiro, R. M.; Toh, M.; Carvalho, A.; Kloc, C.; Castro Neto, A. H.; Eda, G. Origin of Indirect Optical Transitions in Few-Layer MoS₂, WS₂, and WSe₂. *Nano Lett.* **2013**, *13* (11), 5627–5634.
- (17) Tonndorf, P.; Schmidt, R.; Böttger, P.; Zhang, X.; Börner, J.; Liebig, A.; Albrecht, M.; Kloc, C.; Gordan, O.; Zahn, D. R. T.; Michaelis de Vasconcellos, S.; Bratschitsch, R. Photoluminescence Emission and Raman Response of Monolayer MoS₂, MoSe₂, and WSe₂. *Opt. Express* **2013**, *21* (4), 4908–4916.
- (18) Chen, P.; Atallah, T. L.; Lin, Z.; Wang, P.; Lee, S.-J.; Xu, J.; Huang, Z.; Duan, X.; Ping, Y.; Huang, Y.; Caram, J. R.; Duan, X. Approaching the Intrinsic Exciton Physics Limit in Two-Dimensional Semiconductor Diodes. *Nature* **2021**, *599*, 1–7.
- (19) Uddin, S. Z.; Rabani, E.; Javey, A. Universal Inverse Scaling of Exciton-Exciton Annihilation Coefficient with Exciton Lifetime. *Nano Lett.* **2021**, *21* (1), 424–429.
- (20) Lee, Y.; Forte, J. D. S.; Chaves, A.; Kumar, A.; Tran, T. T.; Kim, Y.; Roy, S.; Taniguchi, T.; Watanabe, K.; Chernikov, A.; Jang, J. I.; Low, T.; Kim, J. Boosting Quantum Yields in Two-Dimensional Semiconductors via Proximal Metal Plates. *Nat. Commun.* **2021**, *12* (1), 1–9.
- (21) Abakumov, V. N.; Perel, V. I.; Yassievich, I. N. *Nonradiative Recombination in Semiconductors*; Elsevier: Amsterdam, 1991.
- (22) Toyozawa, Y. On the Dynamical Behavior of an Exciton. *Progr. Theoret. Phys. Suppl.* **1959**, *12*, 111–140.
- (23) Wang, G.; Marie, X.; Bouet, L.; Vidal, M.; Balocchi, A.; Amand, T.; Lagarde, D.; Urbaszek, B. Exciton Dynamics in WSe₂ Bilayers. *Appl. Phys. Lett.* **2014**, *105* (18), 182105.
- (24) Kumar, S.; Kaczmarczyk, A.; Gerardot, B. D. Strain-Induced Spatial and Spectral Isolation of Quantum Emitters in Mono- and Bilayer WSe₂. *Nano Lett.* **2015**, *15* (11), 7567–7573.
- (25) Kulig, M.; Zipfel, J.; Nagler, P.; Blanter, S.; Schüller, C.; Korn, T.; Paradiso, N.; Glazov, M. M.; Chernikov, A. Exciton Diffusion and Halo Effects in Monolayer Semiconductors. *Phys. Rev. Lett.* **2018**, *120* (20), 207401.
- (26) Cordovilla Leon, D. F.; Li, Z.; Jang, S. W.; Cheng, C.-H.; Deotare, P. B. Exciton Transport in Strained Monolayer WSe₂. *Appl. Phys. Lett.* **2018**, *113* (25), 252101.
- (27) Uddin, S. Z.; Kim, H.; Lorenzon, M.; Yeh, M.; Lien, D.-H.; Barnard, E. S.; Htoon, H.; Weber-Bargioni, A.; Javey, A. Neutral Exciton Diffusion in Monolayer MoS₂. *ACS Nano* **2020**, *14* (10), 13433–13440.
- (28) Lien, D.-H.; Amani, M.; Desai, S. B.; Ahn, G. H.; Han, K.; He, J.-H.; Ager, J. W., 3rd; Wu, M. C.; Javey, A. Large-Area and Bright Pulsed Electroluminescence in Monolayer Semiconductors. *Nat. Commun.* **2018**, *9* (1), 1229.
- (29) Cho, J.; Amani, M.; Lien, D.; Kim, H.; Yeh, M.; Wang, V.; Tan, C.; Javey, A. Centimeter-scale and Visible Wavelength Monolayer Light-emitting Devices. *Adv. Funct. Mater.* **2020**, *30* (6), 1907941.
- (30) Withers, F.; Del Pozo-Zamudio, O.; Schwarz, S.; Dufferwiel, S.; Walker, P. M.; Godde, T.; Rooney, A. P.; Gholinia, A.; Woods, C. R.; Blake, P.; Haigh, S. J.; Watanabe, K.; Taniguchi, T.; Aleiner, I. L.

Geim, A. K.; Fal'ko, V. I.; Tartakovskii, A. I.; Novoselov, K. S. WSe₂ Light-Emitting Tunneling Transistors with Enhanced Brightness at Room Temperature. *Nano Lett.* **2015**, *15* (12), 8223–8228.

(31) Sun, Y.; Wang, D.; Shuai, Z. Indirect-to-Direct Band Gap Crossover in Few-Layer Transition Metal Dichalcogenides: A Theoretical Prediction. *J. Phys. Chem. C* **2016**, *120* (38), 21866–21870.

Recommended by ACS

Ultralocalized Optoelectronic Properties of Nanobubbles in 2D Semiconductors

Sara Shabani, Abhay N. Pasupathy, *et al.*

SEPTEMBER 19, 2022
NANO LETTERS

READ 

Positively Charged Biexcitons in Monolayer WSe₂ in Type-I GaSe/WSe₂ van der Waals Heterostructures: Implications for the Biexciton Laser

Jiajun Chen, Chunxiao Cong, *et al.*

JULY 21, 2022
ACS APPLIED NANO MATERIALS

READ 

Boosting Exciton Transport in WSe₂ by Engineering Its Photonic Substrate

Quanbing Guo, Hongxing Xu, *et al.*

JULY 25, 2022
ACS PHOTONICS

READ 

Utilizing Ultraviolet Photons to Generate Single-Photon Emitters in Semiconductor Monolayers

Wei Wang, Xuedan Ma, *et al.*

DECEMBER 14, 2022
ACS NANO

READ 

Get More Suggestions >